ARMY RESEARCH LABORATORY

Scintillation Spectroscopy for Detection of Depleted Uranium

by J. T. Mlack and M. S. Litz

ARL-TR-4990 **September 2009**

NOTICES

Disclaimers

The findings in this report are not to be construed as an official Department of the Army position unless so designated by other authorized documents.

Citation of manufacturer's or trade names does not constitute an official endorsement or approval of the use thereof.

Destroy this report when it is no longer needed. Do not return it to the originator.

Army Research Laboratory
Adelphi, MD 20783-1197

ARL-TR-4990 **September 2009**

Scintillation Spectroscopy for Detection of Depleted Uranium

J. T. Mlack and M. S. Litz
Sensors and Electron Devices Directorate, ARL

REPORT DOCUMENTATION PAGE	Form Approved OMB No. 0704-0188

PLEASE DO NOT RETURN YOUR FORM TO THE ABOVE ADDRESS.

1. REPORT DATE *(DD-MM-YYYY)*	2. REPORT TYPE	3. DATES COVERED (From - To)
September 2009	Summary	July–September 2008

4. TITLE AND SUBTITLE

Scintillation Spectroscopy for Detection of Depleted Uranium

5a. CONTRACT NUMBER

5b. GRANT NUMBER

5c. PROGRAM ELEMENT NUMBER

6. AUTHOR(S)

J. T. Mlack and M. S. Litz

5d. PROJECT NUMBER

5e. TASK NUMBER

5f. WORK UNIT NUMBER

7. PERFORMING ORGANIZATION NAME(S) AND ADDRESS(ES)

U.S. Army Research Laboratory
ATTN: RDRL-SED-E
2800 Powder Mill Road
Adelphi, MD 20783-1197

8. PERFORMING ORGANIZATION REPORT NUMBER

ARL-TR-4990

9. SPONSORING/MONITORING AGENCY NAME(S) AND ADDRESS(ES)

10. SPONSOR/MONITOR'S ACRONYM(S)

11. SPONSOR/MONITOR'S REPORT NUMBER(S)

12. DISTRIBUTION/AVAILABILITY STATEMENT

Approved for public release; distribution unlimited.

13. SUPPLEMENTARY NOTES

14. ABSTRACT

This report describes the use of Sodium Iodide (NaI) scintillation detectors, for the detection of Depleted Uranium (DU) at long ranges with short integration times. Experimental data was taken by setting up the NaI detector in front of a 16 kg sample of DU and looking at the variations in the observed decay spectrum over different distances, integration times, and detector orientation. Also, using a known efficiency equation for NaI detectors, an analytical comparison of measured to calculated data was performed. This report is meant to serve as a basis for future DU detection experiments by providing base measurements and predictions for further studies.

15. SUBJECT TERMS

NaI Scintillator, radiation sensor

16. SECURITY CLASSIFICATION OF:			17. LIMITATION OF ABSTRACT	18. NUMBER OF PAGES	19a. NAME OF RESPONSIBLE PERSON
a. REPORT	b. ABSTRACT	c. THIS PAGE			M. S. Litz
Unclassified	Unclassified	Unclassified	UU	44	19b. TELEPHONE NUMBER (*Include area code*) (301) 394-5556

Standard Form 298 (Rev. 8/98)
Prescribed by ANSI Std. Z39.18

Contents

List of Figures

List of Tables

1. Introduction/Background

Today's military uses Depleted Uranium (DU) in armor piercing munitions as well as armor plating. This is because the density is almost twice that of lead, 19 g/cm^3 versus 11.34 g/cm^3. Recovery of DU-containing rounds and materials is important for environmental, experimental, and health concerns. DU when used in an armor piercing round, can ignite upon impact and release Uranium particles into the air. Although the beta particle radiation that uranium releases cannot pass the skin, the internal organs have no protection, making inhalation and ingestion of DU a concern. This concern is even more significant as DU is also chemically toxic.

Naturally occurring Uranium contains roughly 99.3% Uranium 238, where DU is generally composed of 99.8% Uranium 238. This change in composition is what makes the Uranium "Depleted". The reason natural Uranium is important is its use for nuclear weapons and fuel for nuclear reactors. Uranium 235 is required for fission, and is extracted from the natural Uranium, leaving DU as a by-product (*1*). U-238 being the most abundant part of DU, is not only an emitter of beta particles, but gamma-rays as well. While beta particles do not pass through the skin, gamma-rays will pass right through and travel much farther distances. This makes gamma-ray detection the best method of DU detection.

The method used in our experiments for detecting DU was a Sodium Iodide (NaI) scintillation detector. Other radiation detectors exist, such as High Purity Germanium (HPGe), whose detected DU spectrum is seen in figure 1, and Silicon Lithium, whose DU spectrum is not shown. However, NaI is a better choice than HPGe, because it is more sensitive, and requires no cryogen cooling. Silicon drifted Lithium is a poor choice as its gamma-ray detection range is from 0–100 keV, but DU produces gamma-rays of much higher energy. For this application of an easily portable gamma-ray detection system, NaI would be the best initial approach.

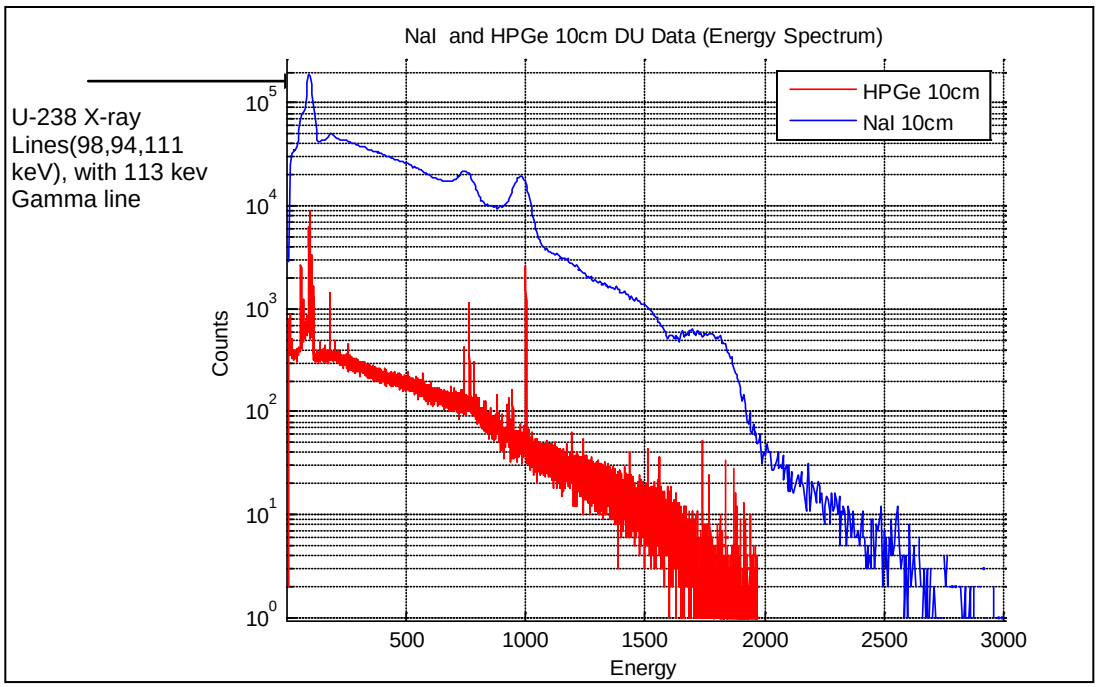

Figure 1. Comparison of DU gamma-ray spectra taken by HPGe and NaI detectors. The graph is of the number of Counts recorded vurses Energy of the counts. The spectrum recorded by the NaI detector is less well-defined but it observes recognizable energy peaks and overall more counts which can be used for data evaluation. Marked are some of the energy peaks used in this report, i.e., the 1001 keV Pa-234 m line and the U-238 X-ray and gamma lines around 94 keV.

A NaI scintillation detector consists of a solid NaI crystal and a Photomultiplier Tube (PMT). The NaI crystal becomes excited by the incident gamma-rays and lumenesces when struck by them. The gamma-ray does not need to strike the front of the detector to activate the crystal. The PMT takes in the light from the crystal and transforms that into a voltage pulse. The light intensity is integrated during a “shaping time”, during which the PMT integrates the optical photons from the crystal. A Multi-channel Analyzer (MCA) separates the pulses, hereafter referred to as counts, into one of many channels based on the pulse height, i.e., energy of the gamma-ray. This sorting by energy forms a gamma-ray spectrum from the counts, as seen in figure 1. By looking at this spectrum after a specified detection time, the radioactive material(s) present, if any are, can be identified. The spectrum displays real-time in the program ScintiVison-32 and its final output is saved for future analysis.

The NaI detector is designed for detection of gamma-ray radiation that comes off of any radioactive material. Every material has its own unique gamma-ray emission spectrum. Figure 1 is the gamma-ray spectrum for the DU sample taken by both an HPGe detector and a NaI detector. Here there are many peaks which represent specific gamma-ray energies that DU's primary component, U-238, releases in its nuclear decay process. Also, some peaks represent the decay of its daughter isotopes (like Thorium 234 and Protactinium 234 m). The highest peak(s) are U-238 K X-Ray peaks (98 & 94 keV), though the 766 keV and 1001 keV Protactinium 234 m peaks are also easy to measure (*2*). Some of the spectrum in figure 1 is from natural background radiation. When background measurements are made in this report, it is when the detector is shielded from our DU target or the DU target itself is covered with lead shielding.

The detection of the gamma-rays is dependent upon the geometry of the detector and radioactive source, as well as the time during which the detector is counting radiation (*3*). Using an equation based on geometry and photon absorption, a calculation can be made of the expected number of counts from the NaI detection system for comparison with experimental data.

For detection of the DU target, we performed four separate parametric studies of the response of the NaI detector. The first test was the NaI detector's response over varying distance from the target, the second over varying detection time, the third was varying angle with respect to the target, and the final was comparing our experimental data to our theoretical calculations. These tests were performed in order to understand the detection distance limitations of the NaI detector, the detection time limitations, effects of detector angular position, and the possibilities and hurdles of using a numerical model to predict future outcomes.

2. Experiments and Calculations

2.1 Basic Experimental Setup

The experimental setup consists of a 3 in diameter by 3 in thick NaI Scintillation Detector (see figure 2) and detection apparatus positioned in our radiation test cell. A DU Collimator inside of Linac x-ray machine serves as the DU target. The apparatus for the detector consists of a small laptop computer installed with ScintiVision-32 software and linked via fiber optics to a computer we use to remotely operate the laptop. Attached to the back end of the detector is an Ortec DigiBase MCA, which transfers the output from the PMT at the base of the NaI crystal by USB to the laptop. The detector's position is manipulated depending on the experiment we are trying to perform.

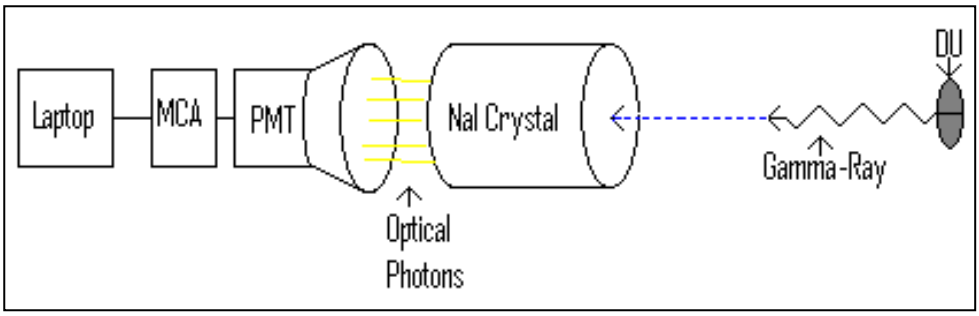

Figure 2. Diagram of the Sodium Iodide detector system. Gamma-rays from a radioactive source excite the NaI Crystal causing optical photons to be released. The photons are gathered and integrated in the PMT. After a specified time, a voltage pulse proportional to the integrated photons is produced. The pulse is sent to the Multi-Channel Analyzer (MCA) where it is binned based on the pulse height. The MCA then sends the binning information to the laptop where it can be viewed real-time.

Our standard procedure is to calibrate the detector before each experiment, or set of data collections. This calibration is performed using small, quarter-sized, 1 microCurie, check sources. Each check source contains a specific radioisotope. Knowing the characteristic gamma-ray energies of these check sources, an energy calibration line fit is created for the channels which the MCA bins each gamma-ray into. By comparing an unknown gamma-ray peak in our spectrum to the calibrated energies, a gamma source can be identified. The calibration is performed using seven check sources containing Ba-133, Cd-109, Na-22, Mn-54, Co-57, Co-60, and Cs-137. For calibration, the sources are individually placed 8 in from the front of the detector. The detection integration time used for calibration is 15 min in order to get an accurate spectrum of each isotope.

2.2 Distance Experiments

The first experiment performed measured the DU spectrum as a function of distance with a detection time of 3 min. The 3 min integration time was chosen in order to better simulate how much time our detector might have to sit in an area and search for radiation. The reason this test was performed was to look at how far away we were able to detect the DU target in the test cell. If the target could be seen from the farthest point the test cell allowed, we would then try to extrapolate how far away the detector might be able to see DU if given more space. The NaI detector was set up on a moveable cart between two cinderblocks for the first test, and two lead bricks for the second (see figure 3). The blocks were used in order to support the detector and to orient it as closely as possible with the center of the DU target. The 3 min detection runs were started at approximately 1 centimeter (cm) from the DU and increased to 10 cm, 20 cm, 50 cm, 90 cm, 200 cm, 500 cm, and 1000 cm. The data was then compiled using code written for the mathematical analysis software MATLAB. The code plots the spectrum recorded at each distance, rolling in the detector calibration, performed before the test. Large dead times were measured during the first set of measurements. Dead time is detection time during which the

detector is busy analyzing a signal from a gamma-ray and thus cannot analyze another incoming gamma-ray. This is caused by large numbers of incoming gamma-rays. Dead time less than 15% is a reasonable number. Detections with larger dead times were discounted during the analysis of this experiment as not statistically valid.

Figure 3. Picture of the setup for distance detection of DU. Detector and equipment are located in bottom right of picture. DU target located in upper left. Test was performed to find out the maximum detection distance of the NaI detector.

2.3 Time Experiments

Another aspect in detection of DU is how much time is needed to determine the presence of DU. In order to observe this with our NaI detectors we varied the detection integration time. Starting with an integration time of 30 min, we decreased the time to 3 min, 2 min, 1 min, 30 s, and 15 s. This gave us a basis for understanding the time-based limitations of our detector. The setup for this experiment involved leaving the NaI detector at the 1000 cm distance mark, pointed at the DU, and then decreasing the detection time. For comparison, using the same time steps, we rotated the detector 180 degrees and placed a half inch thick lead plate behind the detector in order to produce a "background" condition. Even further, for a more accurate zero background, the detector was completely covered inside a two inch thick lead enclosure. This was done in order to cut out as much background radiation as possible, again with the same time step detections being run. Pictures of this setup are displayed in figure 4.

(a)

(b)

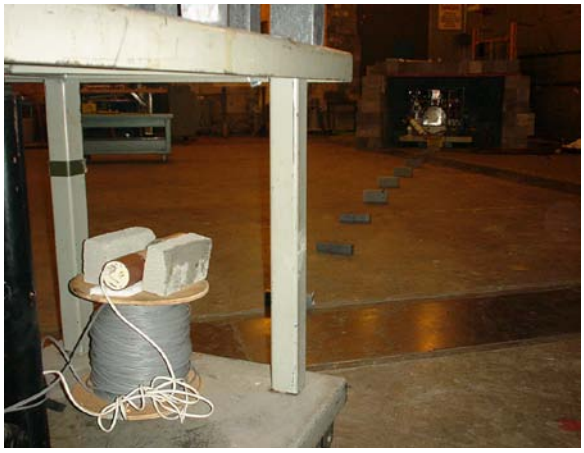

(c)

Figures 4. Pictures of the 10 mr setup for Time experiment. (a) Detector facing away from the DU with the half inch thick lead plate behind it. (b) The detector encased in 2 in thick lead bricks. The detector facing the DU. Test was performed to find a minimum detection time for DU at long distance.

2.4 Direction Experiment

In order to look at the DU spectrum while only the front face of the detector is open and on target, we performed a third test based on detector direction. We first setup the NaI detector 5 m from, and level with, the DU target. The detector was started off with the front end of the detector facing directly at the DU target. A detection run of 3 min was then performed, after which the detector was rotated 45 degrees counter clockwise. The rotation was performed a total

of eight times with 0 degrees defined as facing directly at the DU target and 180 degrees being directly away. However, knowing that the detector is subject to background from all directions it was placed in tube of lead, eighth of an inch thick, with only the front of the detector exposed. This way we could better understand the difference in spectrum from varying the degree of rotation with respect to target. Separate detection runs with the detector not shielded in the lead tube were also performed for comparison. Pictures of this setup are shown in figure 5.

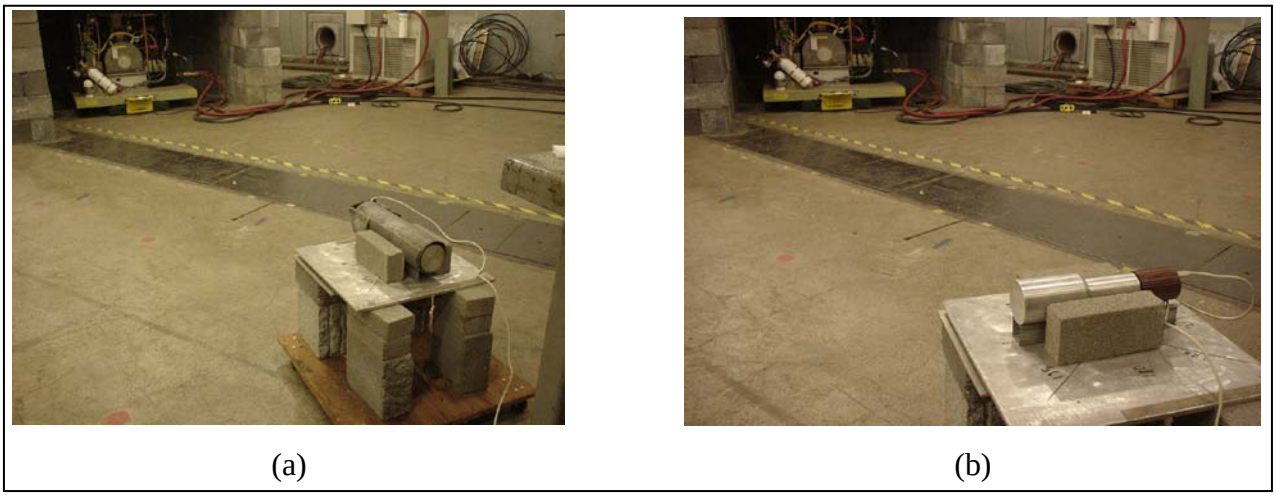

(a) (b)

Figure 5. (a) The NaI detector shielded by an eighth inch thick lead jacket, all except the detector face, for the Direction testing at 5 m from the DU target. (b) The unshielded detector for the Direction testing. This test was performed to understand the effects of lead shielding and direction to source on the NaI detector.

2.5 Calculations

The main calculation performed was for the efficiency of NaI detectors in detecting gamma radiation. The integral for this calculation is located in Heath (*3*), but is also shown in figure 6. The equation is derived from the geometry of the detector and its relationship to the location of the source as well as the absorption coefficient of the detector material. The values for the absorption coefficient were obtained from Evans (*4*). The integral makes the assumption that the source we are looking at is a point source, which it is not. For our farther measured distances and as a starting calculation, it provides a good initial estimate.

In order to make the efficiency calculations useful, we needed to calculate the decay of the source. The process of calculating the counts expected from the radiation source (i.e., the number of gamma-rays coming of the source), starts with the radioactivity of the DU target, which is 11 micro-curies. The radioactivity was then decreased in accordance with the 4.46 billion year half-life of U-238. That number then needed to be converted to becquerels, or decays per second. Each isotope, also having its own unique gamma-ray spectrum, has characteristic intensities for each of its primary gammas that it produces, which are well recorded and documented (*5*). The intensity is measured in gammas of a defined energy per 100 decays of an isotope. Knowing the decay of the isotope, the intensity of the desired gamma-ray, and the

detection time, one can calculate the amount of counts that should be detected in that energy's peak in the experimental gamma ray spectrum.

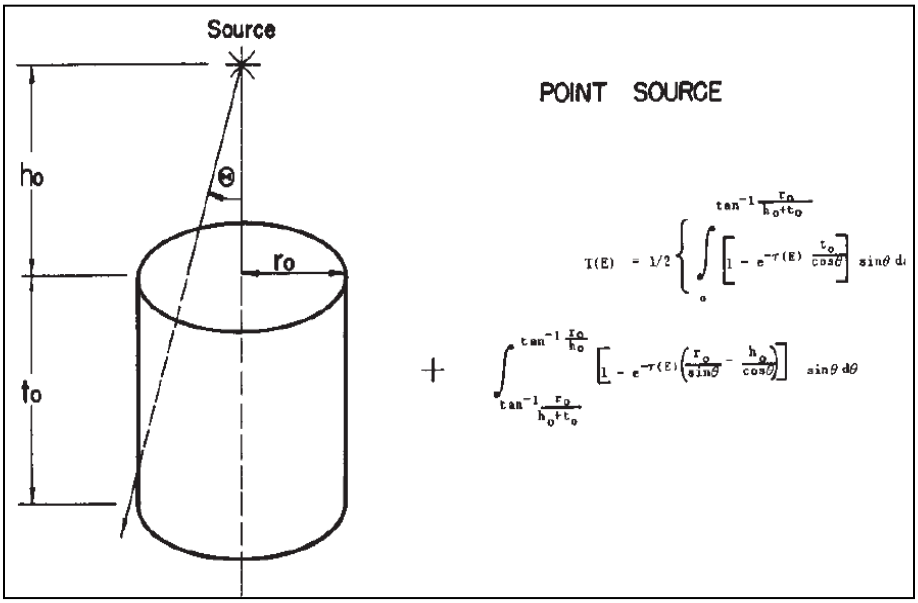

Figure 6. Equation for Efficiency of a Sodium Iodide Detector looking at a point source of radiation, taken from *Spectrometry: Gamma-Ray Spectrum Catalogue*. h0 is the distance from source to detector, t0 is detector length, r0 is detector radius, T(E) is efficiency, and τ (E) is absorption coefficient of NaI based on gamma-ray energy (*3*).

3. Methode of Data Analysis

All data obtained from ScintiVision-32 were analyzed using code written in Matlab analysis software. The codes, which are located in Appendix A of this report, are primarily designed to bring in the data from ScintiVision-32 output files and plot the recorded spectrum as well as any other desired information. The analysis focussed on (a) the total number of counts recorded by the detector, (b) the number of counts in the highest peak of the spectrum, and c) the location of the highest peak of the spectrum in comparison to the energy calibration.

Although the total number of counts is indiscriminant as to what kind of radioactive source the detector is looking at, this number is useful in a detector when the primary concern is the presence of radioactive materials without discriminating what type (i.e., is there a radioactive source nearby). An increase in total counts should correspond to the detector coming closer to a gamma producing source. When using total counts as the discriminating factor, knowledge of typical background counts is essential.

The number of counts in the highest peak is also a factor in determining changing proximity to a source. Analysis of the location of the highest peak can be used as a discriminating factor,

beyond Total Counts, as to what radioactive source(s) is (are) present. Knowing the characteristic lines of a certain isotope and comparing them to the location of the highest peak, after the detector is calibrated, will tell if a desired source is close by.

Finally, fitting curves to Total Counts and counts in highest peak, allows predictions to be made on the effects on altering distance from the source, detection time, and direction with respect to the source. These predictions can then give insight into the viability of further experiments. The method of error and deviation for these analyses is based on those detailed in Chapter 3 of Knoll (*6*). Since the tests were performed a limited number of times, the section on "Estimation of the Precision of a Single Measurement" forms the basis of the data evaluation. The main component of this section that was used in this report was the use of the square root of a single measurement as an estimate for standard deviation.

4. Results and Discussion

4.1 Distance Experiment Results

Figure 7 shows the DU spectrum as detected by the NaI detector on 18 May 2007 over increasing distance. The peaks in the graph are the combined U238 X-ray lines (94, 98, 111 keV), combined with a 113 keV gamma-ray line, as well as the 1001 keV Pa-234m gamma-ray line.

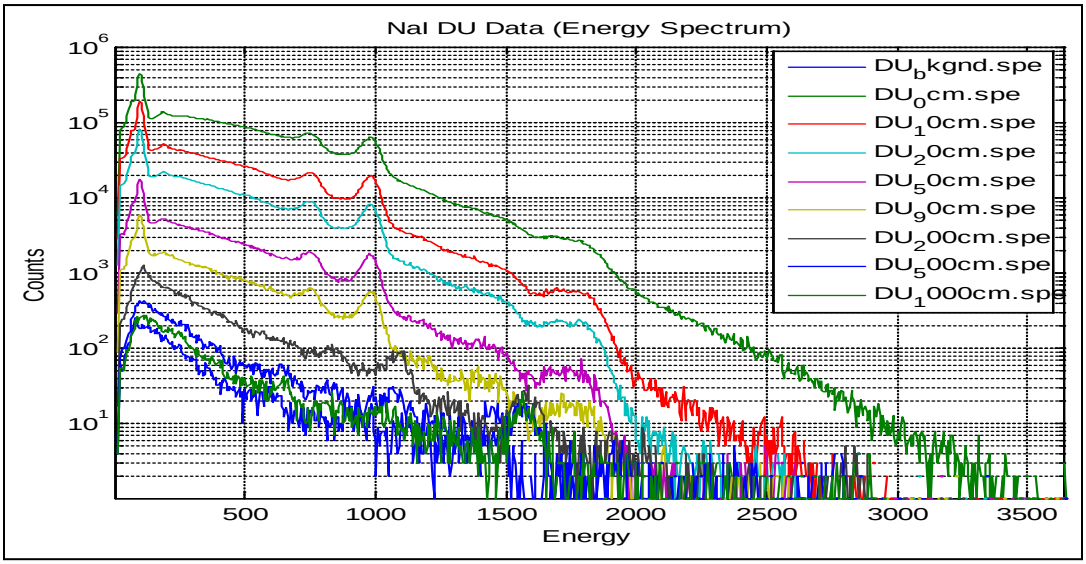

Figure 7. Graph of spectrum detected by NaI detector for the minute detection runs over increasing distance with peaks at approximately 94 keV and 1000 keV, the highest peak being the 94 keV peak.

As distance from the sources increases the signal of the DU drops off significantly. The signal at 10 m looks more like background than DU. The graph in figure 11 shows the graphs of the number of counts in the highest peak and Total Counts of the spectrum over distance. Figure 8 also shows the total of the background counts as well as the counts in the highest background peak as straight lines. The highest peak in the spectrums is around 94 keV. When the measured counts fall to background levels, the detector no longer has useful detection range and no detection information can be deduced. At around 10 m, the measured data is approaching the background limit. The results looking at Total Counts and Highest Peak Counts versus the highest peak counts in background and the total background counts are displayed in table 1.

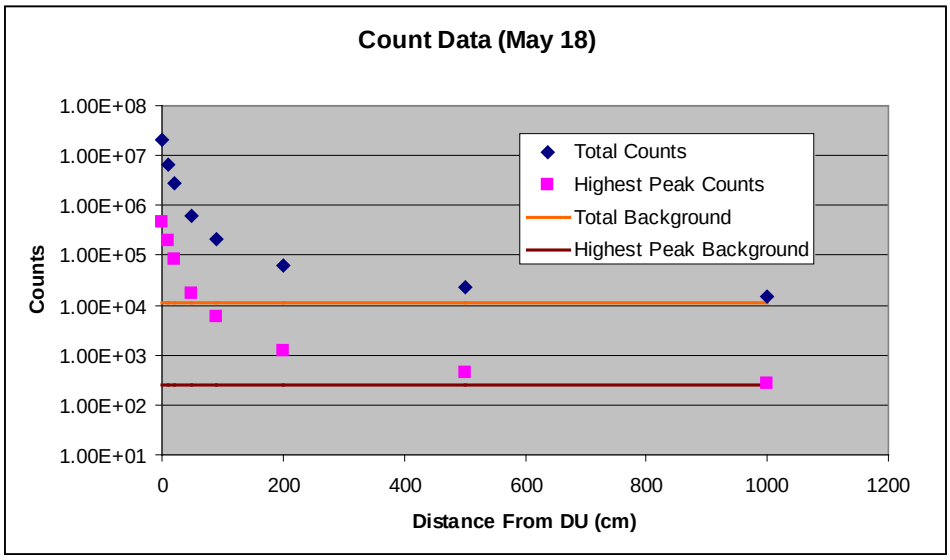

Figure 8. Graph of total counts and counts in the highest peak (highest peak counts) over distance as well as lines depicting the values for a background measurement. Although at 10 m the counts fall seem to fall into background, analysis of the numbers themselves, table 1, show that there is still a significant difference.

Table 1. Data was extracted from the 10 m results of figure 7, with their respective standard deviations. This specific data shows that even as far away as 10 m there is still a significant difference between DU and background for at least total counts. However, for highest peak counts, the deviations overlap, making highest counts a poor choice for determination of a radioactive source at 10 m.

	Counts Recorded	Std. Dev. Estimate
Total Counts	15154	123.1015841
Total Counts of Bkgnd	11395	106.7473653
Highest Peak Counts	271	16.46207763
Highest Peak Cnts. Bkgnd	251	15.84297952

There is a measurable difference in the number of counts. Using the estimate for standard deviation, i.e., the square root of the counts value, we find that the difference between Total Counts and background falls well outside one standard deviation of each other, as shown in table 1 (*6*).

However, this is not the case for Highest Peak Counts. This means that by looking at Total Counts of a spectrum we can differentiate background from DU from at least 10 m. However, Highest Peak Counts can only be used from at least 5 m.

From the data from figure 8 an estimate can be made of how far out the detector might be able to detect the DU. By fitting a line of Total Counts and Highest Peak Counts, minus their respective backgrounds, the data can be evaluated for larger distances. Figure 9 shows the fitted curves and table 2 shows the curves evaluated for 20, 35, and 50 m, respectively. Due to a large dead time for the first set of data, we are disregarding the first point at roughly 1 cm from the source.

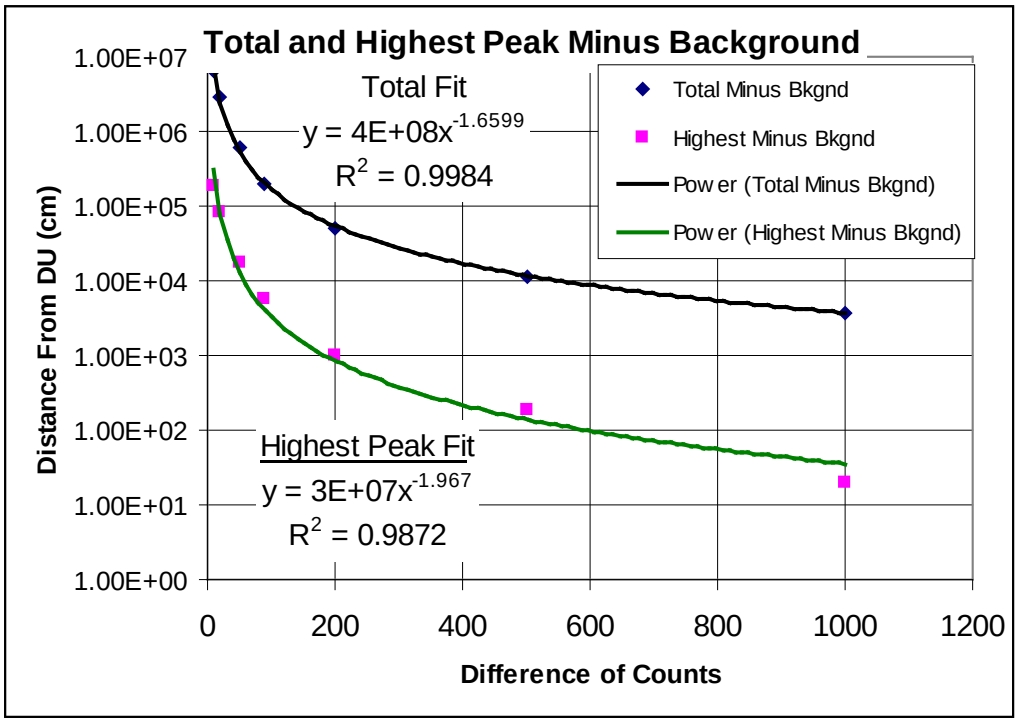

Figure 9. Graph of total and highest peak counts minus observed background with fitted power laws. By evaluating the equations from the fitted lines it is possible to extrapolate to further distances.

Table 2. Estimations of counts for further distance measurements for the decreasing difference between total counts and total background as well as highest peak counts and highest peak background. The predictions show that it may be possible to detect the presence of our DU target from at least 20 m, possibly farther, with a 3 min detection time. The data from the furthest point, 10 m, is also shown for comparison.

	Distance Estimations	
Distance (meters)	**Total Count Difference**	**Highest Peak Difference**
20	1326.417679	9.638184892
35	523.915738	3.205822048
50	289.8275603	1.589451411
Furthest Data Taken		
10	3759	20

Table 2 shows that using the curve fit for Total Counts evaluated at 20 m, there is still a difference larger than two times the standard deviation of Total background. This means that there is a possibility that should further tests be conducted, a detection range of the DU at 20 m from the detector could be achieved.

4.2 Time Experiment Results

At 10 m the best detection test is looking at Total Counts. Thus it was the method used for the 10 m tests over varied time. These results are shown in figure 10, along with lines fitted to the data.

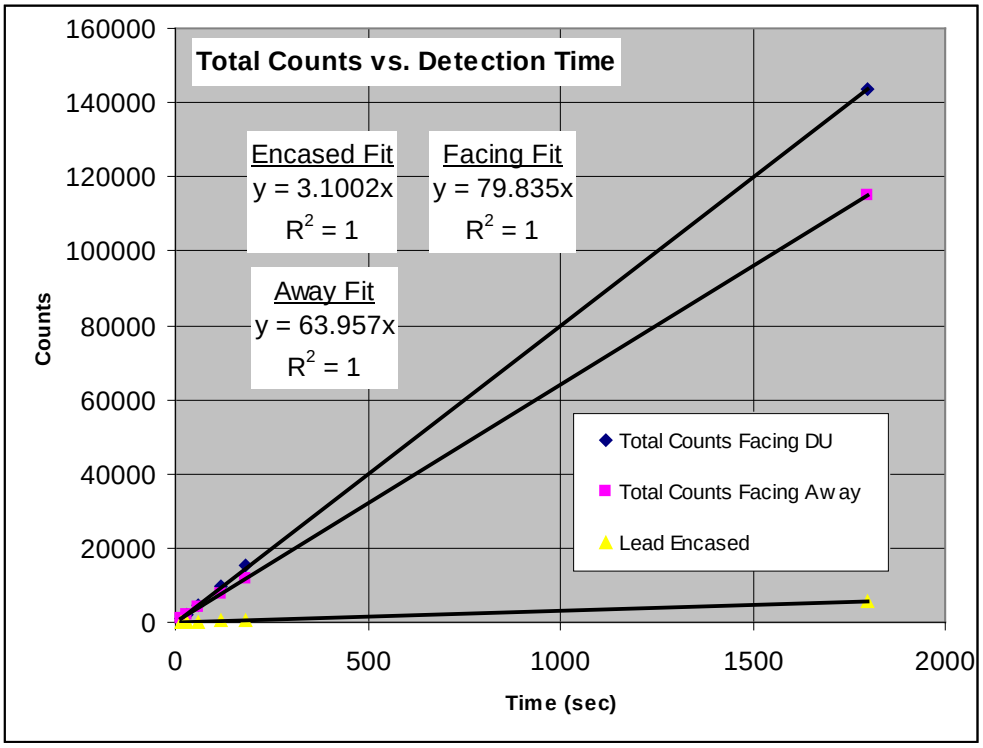

Figure 10. Graph of total counts versus detection time for the time experiment. The data was fitted in order to obtain equations for predictions of minimum total counts measurement time at 10 m.

As would be expected, the number of counts increases linearly with time. Table 3 shows the differences between Facing DU, Away From DU, and Lead Encased. For the 15 s run, the count difference between Facing DU and Away From DU is greater than their standard deviations. This means that at a 15 s integration time, the presence of something radioactive can be determined. Looking at Lead Encased compared to the other measurements, the Facing DU and Facing Away measurements become more significant and would allow for further decreased detection time. The straight line fit to this data reveals (see table 4) that these differences would still be observable at as low as a 10, or possibly 5, second detection time.

Table 3. Time experiment data based on total Counts in spectrum for varying time. Since the difference of total counts facing DU and facing away is much greater than the combined statistical error of both measurements, a 15 s integration time could be used for 10 m detection.

Time (sec)	Total Counts Facing DU	Total Counts Facing Away	Lead Encased
15	1216	1020	38
30	2290	1913	89
60	4794	3912	179
120	9631	7776	381
180	15154	11975	560
1800	143623	115066	5580
Shortest Run (sec)	Facing Std. Dev.	Away Std. Dev	Encased Std. Dev.
15	34.87119155	31.93743885	6.164414

Table 4. Estimations based upon fitted lines of figure 10. Standard deviation is also shown to compare possible statistical overlap. Since two sigma may cause overlap between total counts of facing DU and facing away for predictions for 10 and 5 s detection time, those times would not be precise enough for our application. However, as is shown in table 3, 15 s still provided a difference in counts such that there is still a significant difference between looking at and looking away from the DU.

	Estimations		
Time (sec)	Total Counts Facing DU	Total Counts Facing Away	Lead Encased
10	798.35	638.62	31.002
5	399.175	319.31	15.501
	Std. Dev.	Std. Dev.	Std. Dev.
10	28.25508804	25.27093192	5.567944
5	19.97936435	17.86924733	3.937131

4.3 Direction Experiment Results

Figures 11 through 14 show the results from the Direction Experiments. Specifically figures 11 and 12 show polar plots of the data recorded for Total Counts. Both graphs in figures 11 and 12 show decreasing counts as the angle between the detector face and DU target increases.

However, the total number of counts is significantly decreased due to the lead jacketing which blocks out more than 50% of the radiation detected, when the lead jacket, is an eighth inch thick lead tube covering the detector with only the front face of the detector not covered (see figure 5). The lead does decrease the counts, but it also increases the difference between facing towards the DU and facing away from it. In figure 11, the rotation of the shielded detector changes the number of total counts by 1/3, whereas for the unshielded rotation, figure 12, counts are decreased only by roughly 2/7.

For counts in highest peak there is again a definite drop in the number of counts as the shielded detector is rotated. The decrease is consistent and significant. In this case, a decrease of roughly 1/2 as the detector is rotated from facing to facing away, figure 12a. However, for the highest peak counts for the unshielded rotation, figure 12b, although there is a decrease in counts, the decrease is not consistent as the detector is rotated. At 315 degrees away from the DU target, the number of counts in the highest peak is actually greater than when the detector is facing the DU. The addition of a lead jacket, as far as counts go, has increased the detectors sensitivity. By blocking out sources coming from directions which are not being focused on, the accuracy in determining the location of a source and the difference between it and a "background" increases. The location of the highest peak is also susceptible to the direction of the detector; figures 13a and 13b show the calibrated energy at which the highest peak was located for each directional measurement. The figure for the unshielded detector, although not constant, still varies around a 14 keV wide region. However, for the shielded detector, the region is slightly larger than 30 keV in width and drops sharply after the first measurement which was directly facing the DU target. This shows that during the rotation of the detector there was a clear change in what radiation the detector was looking at, i.e., the shift in location of the highest peak is indicative of moving away from a specific source. The final two direction experiment graphs are the spectrums taken at each angle. The main information to be taken from these graphs is the visual change in the size of the spectrum as the detector is turned. For the lead encased test, figure 14a, the spectrums show large decreases in counts as the angle increases, where as for the unshielded detector, figure 14b, the spectrum stays in relatively the same range for the same increases.

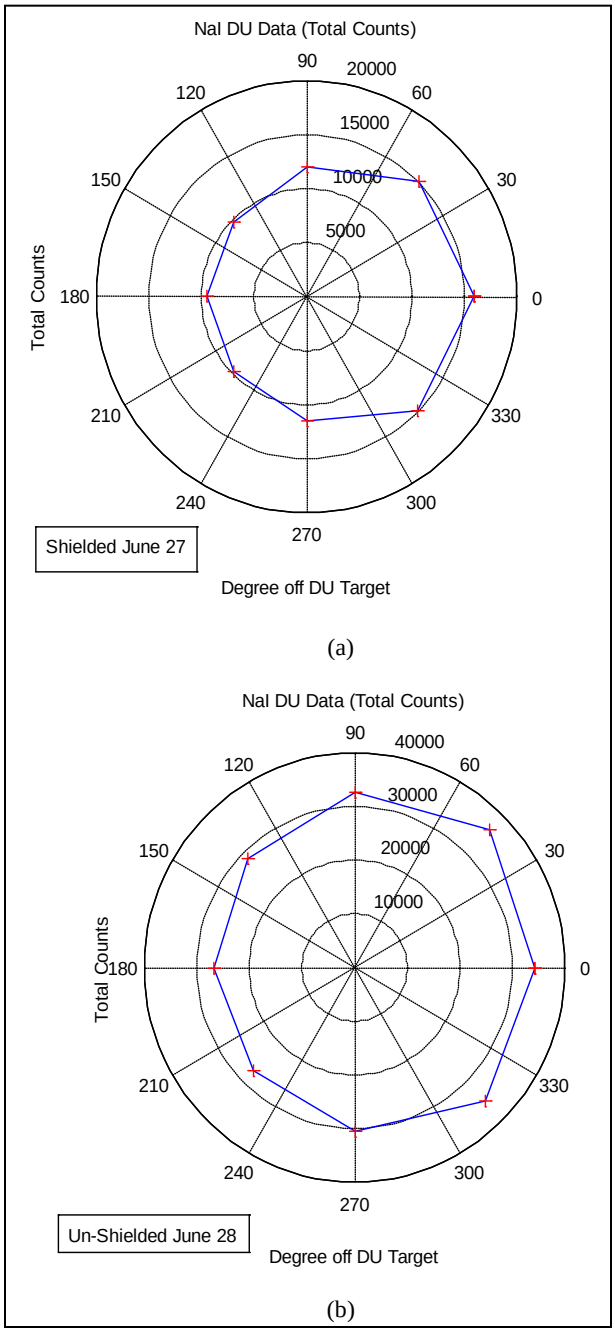

Figure 11. Graphs of total counts versus angle away from DU target at 5 m for 3 min. The graphs illustrate the difference that a lead jacket, and detector facing to source has on results. (a) There is a decrease in counts from front to back, approx. 15,000 to 10,000 counts. (b) The decrease is less drastic, approx. 35,000 to 25,000. This shows lead encasement decrease counts overall, and increases sensitivity to direction to source.

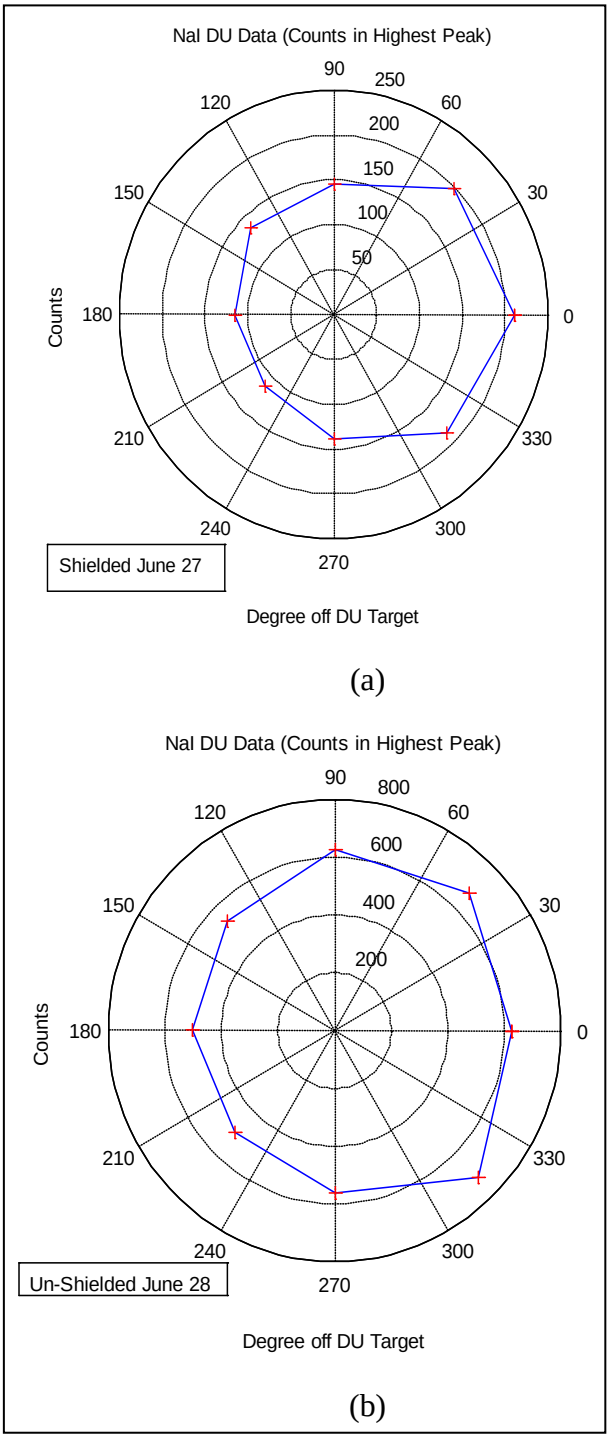

Figure 12. Graphs of the number of counts in the highest peak over angle away from DU target at 5 m away for 3 min. (a) As in figure 11, there is a decrease in counts as direction changes, though there is an unexplained anomaly in (b) at 315 degrees. Again, the changes in counts for the detector shielded by the tube show greater sensitivity to direction than the unshielded.

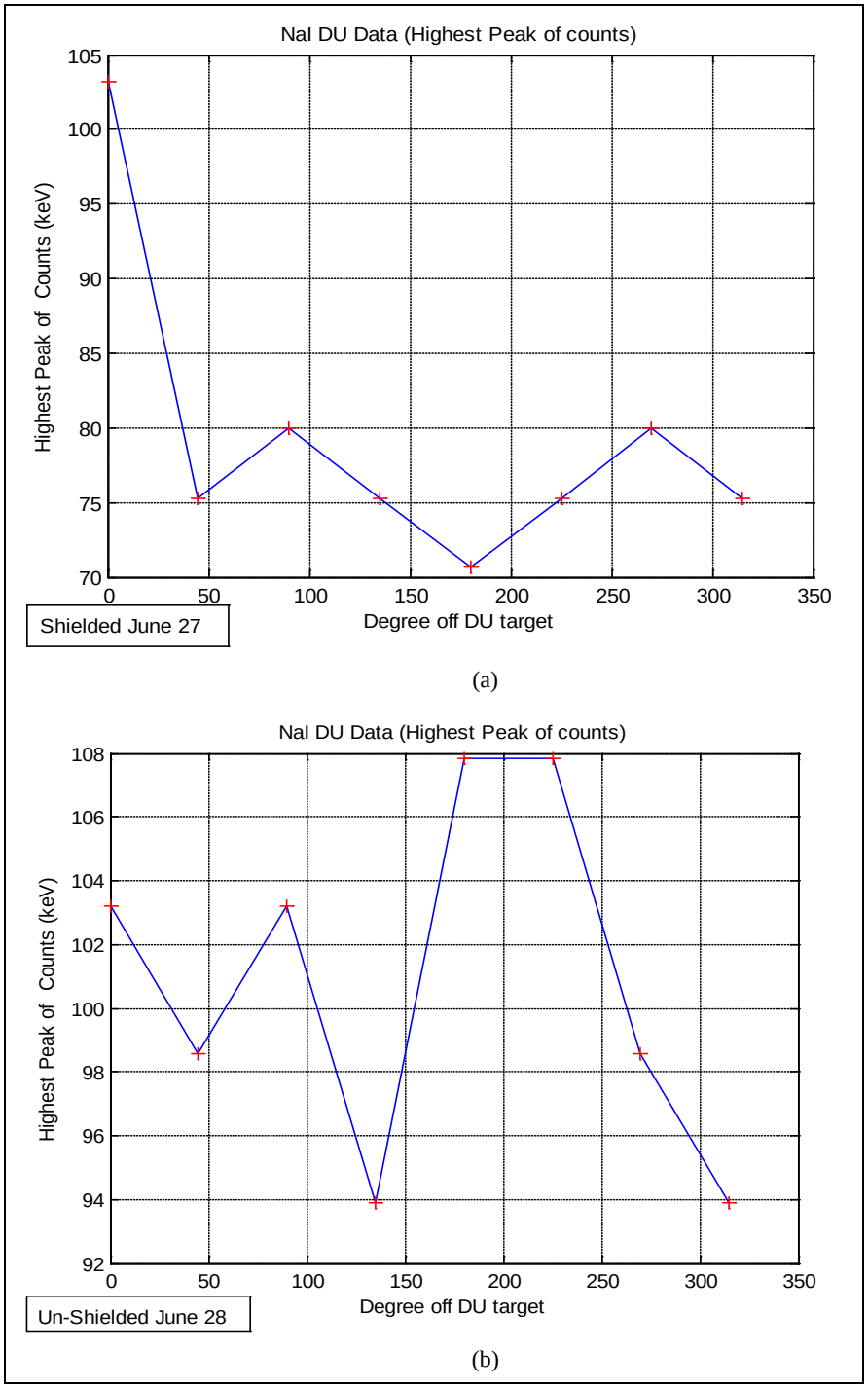

Figure 13. Graphs of location of the highest energy peak based upon calibration over angle away from DU target at 5 m and 3 min detection. (a) Shows a large change in location of the highest peak in the spectrum as the shielded detector is moved off the DU target. (b) There is no definite jump away from a specific energy line, but rather jumps between several. Partial lead shielding seems to help define unique energy lines as the detector is rotated.

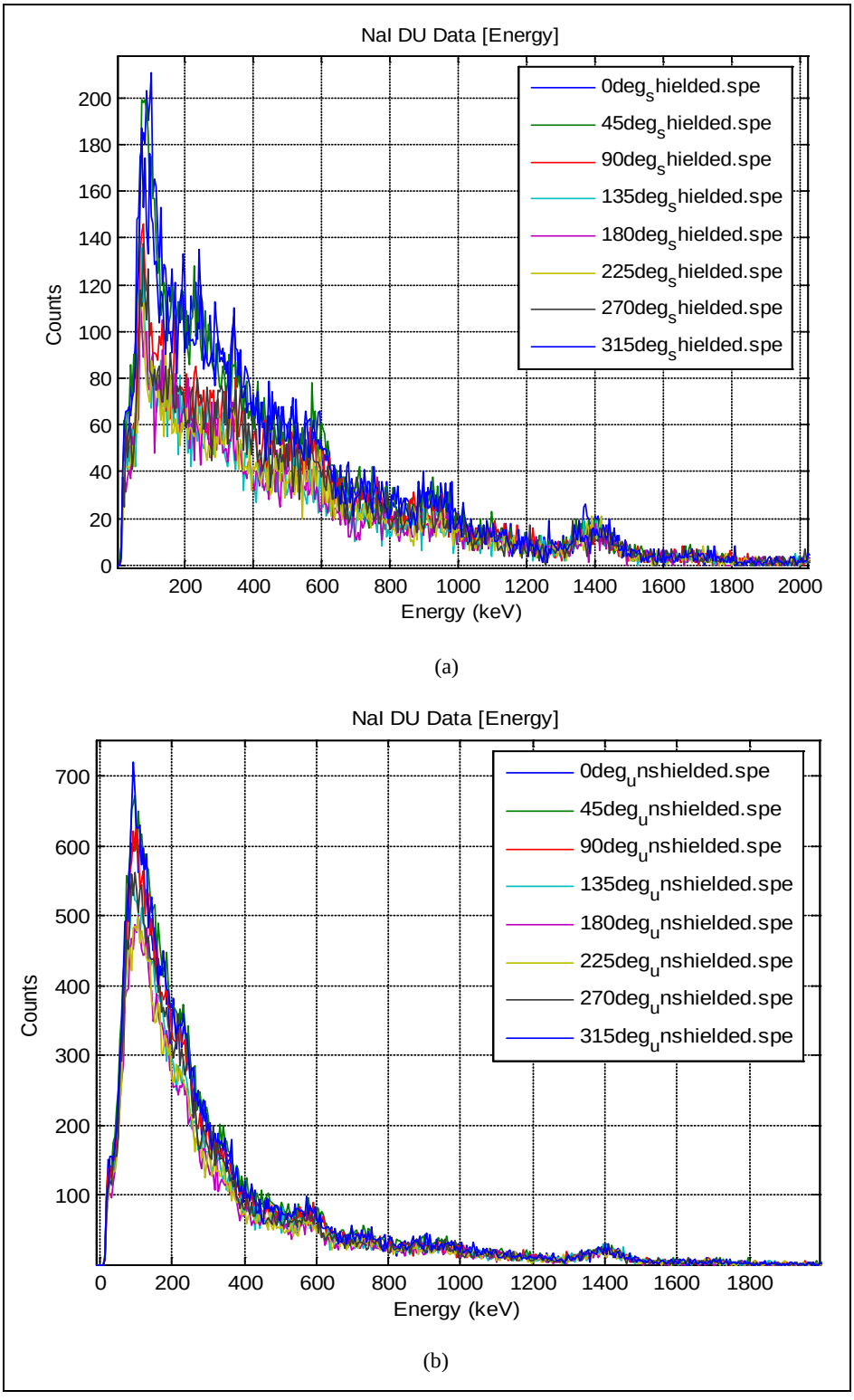

Figure 14. Graphs of energy spectrum, counts over energy, detected by NaI detector. Top graph is shielded detections, bottom is unshielded detections. (a) Each line spectrum was taken at a different angle from the DU target. (b) These figures illustrate the visual difference in moving towards and away from the target. The changes in the shielded spectrum are more visually obvious than the unshielded.

4.4 Efficiency Calculation Results

Figure 15 shows the graphed results from the comparison of the efficiency equation versus the measured counts. For this we observed the 94 keV energy peak as seen in figure 7. Figure 16 shows the output of the integration of the efficiency equation at a distance of 8 in. This is just a raw efficiency, which we calculated for each distance at which we took a measurement with the NaI detector. Although the numbers of our predicted values do not exactly match the calculations, this analysis still serves as an exercise in using known theoretical equations for comparison with experimental results. The differences in the experimental results can be partially explained because the DU target is really not a point source. Also, the equation used only takes into account the absorption of the NaI crystal, and does not account for the possible energy losses in the conversion from gamma-ray to photons or any possible inefficiencies of the PMT, or MCA, or other counting equipment. Knowing these other factors involved in the efficiency equation, however, does give a basis for possibly creating a better equation, or set of equations, that can more properly predict future experiments.

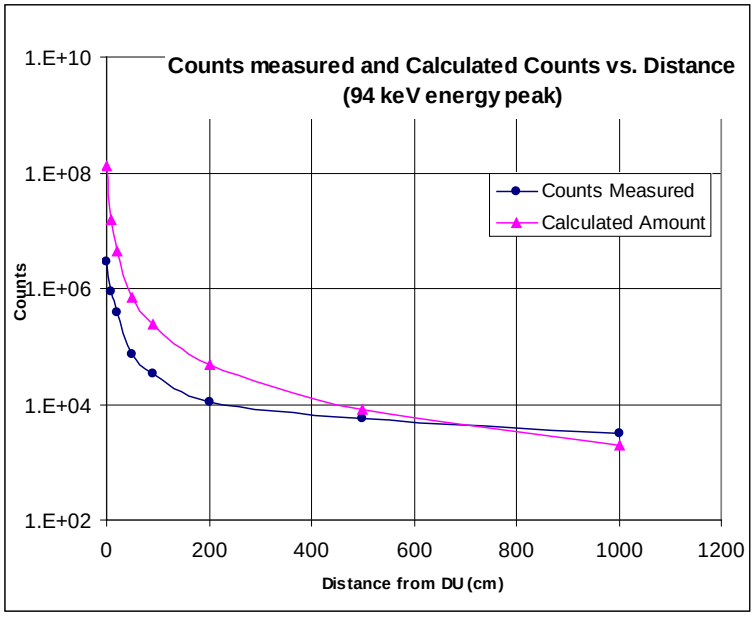

Figure 15. Graph of counts versus distance for predicted number of counts that the NaI detector should detect against the experimental counts measured. The experimental counts came from the number of counts in the 94 keV peaks of figure 7. The predicted counts are based on the efficiency equation from figure 6 as well as the size of the DU target and its known decay process.

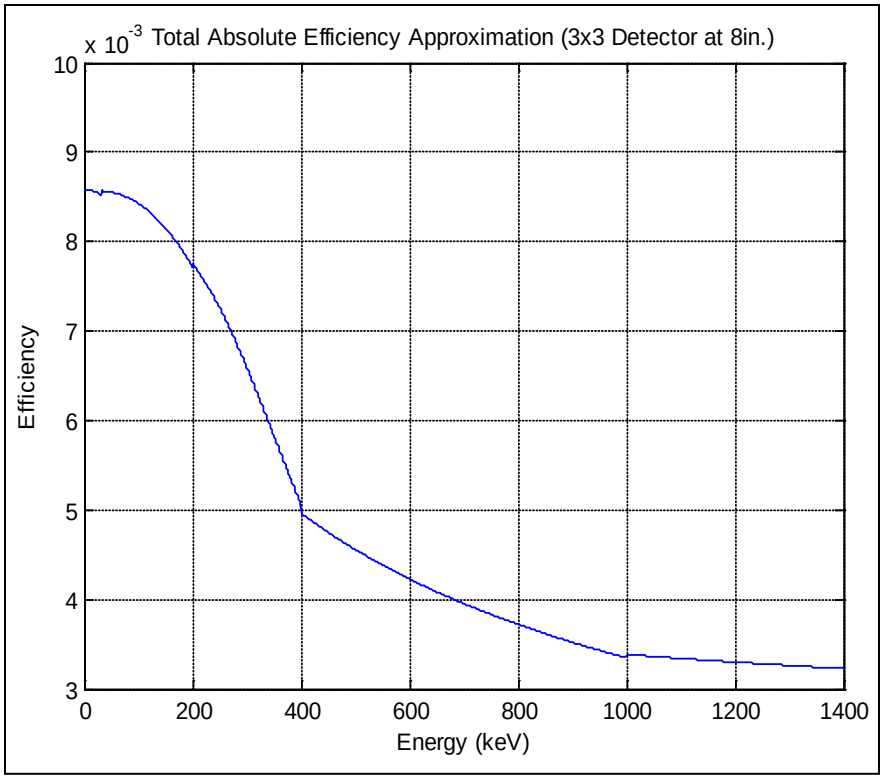

Figure 16. Graph of NaI efficiency for a 3 in by 3 in detector over the energy of incoming gamma-ray. This is the output of a code, attached to the end of this report, written to integrate the equation from figure 6.

5. Summary and Conclusions

The experiments were overall successful in answering the questions that were posed about the details of detecting DU. The distance experiments show that, by using a 3 min detection time, the presence of a radioactive source can be detected from at least 10 m away using changes in the total number of counts as an identifier. Unique identification of an exact isotope species of our size target (11 microCuries) is identifiable at roughly 5 m. Fitting of the experimental data shows a statistically significant (2:1 signal to noise ratio) chance of detecting the DU target from as far away as 20 m using a 3 min detection time.

For the time experiments, (at a distance of 10 m) as low as 15 s for a detection time is sufficient for identifying the presence of a radioactive source, using Total Counts analysis. The fit to the data suggests that this time may be even shorter (as low as 5 s), though as the number counts decreases, the accuracy of the detection decreases.

Finally, the direction experiment suggests that shielding most of the detector, except for the face, can improve the accuracy and methods of detection. This improvement is not only for Total

Counts at long range, and Counts in the highest peak at close range, but also differences in the entire spectra, as well as shifting of the location in the spectrum of the highest peak.

The theoretical calculations and experimental data comparison shows that the current prediction method is insufficient in closely predicting experimental results and requires refinement. By analyzing the operation of the NaI crystal more in-depth it may be possible to account for more of the inefficiencies involved in the detection system. Doing this would allow not only better future prediction on the distance experiments, but possibly also to model even the time and direction experiments.

It must be stressed that these experiments were performed in a shielded room and that each experiment was performed on a different day under different internal environmental conditions. This is why future experiments should realistically combine at least two of the three experiments; this would provide better continuity between the data, as well as a wider range of data. Also, future experiments should include field testing where this setup is going to be normally operated and used.

An important hurdle that should also be noted is variability in size of possible DU targets, from entire tank rounds to small pieces of shrapnel. The absorption of DU of its own gamma radiation is very high and even our detectors will not detect the radiation coming off of each decay of the source. This limits the detection ability of any target. Not only does DU absorb its own radiation, but water, earth, and even metal casing around DU, can decrease the amount of radiation that can be detected.

In the end, a single NaI detector can be used to detect DU or possibly other radioactive sources from fairly long ranges and in short amounts of time. This is under good conditions, but further testing must be done to determine the effect of different more realistic conditions. More work is also required to compile a more accurate and precise numerical model for predicting possible outcomes. Plans are currently to create a detector package to be tested in the field to further study the limitations of NaI detectors themselves in DU detection, as well as the limitations created by environment.

6. References

1. Haslip, D. S.; Cousins, T.; Estan, D.; Jones, T. A. *Field Detection of Depleted Uranium: Final Report of Tasking W284776KR00Z,* Defence Research Establishment Ottawa, DREO TM 2000-049, June, 2000.

2. *Gamma-Ray Spectrum Catalogue: Ge and Si Detector Spectra*, 4th ed., Idaho National Engineering and Environmental Laboratory, September 1998.

3. Heath, R. L. *Scintillation Spectrometry: Gamma-Ray Spectrum Catalogue*, Reissue of IDO-16880, 2nd Ed, Vol. 1(Rev.), February 1997.

4. Evans, R. D. *The Atomic Nucleus*, Mc-Graw Hill Inc., 14th Printing, p. 717, May 1972.

5. Ekström, L. P.; Firestone, R. B. *WWW Table of Radioactive Isotopes*, database version 2/28/99 from URL http://ie.lbl.gov/toi/index.htm.

6. Knoll, G. F. *Radiation and Detection Measurement*, 3rd Ed., John Wiley & Sons Inc., 2000.

7. Keyser, R. M.; Upp, D. L.; Twomey, T. R. *Performance of an HPGe-based and NaI-based Radionuclide Identifier (RIID) in the Identification of Radioactive Materials*, Presented at INMM, July 2005.

8. Coleman, R. L.; Murray, M. E. *Detection of Depleted Uranium in Soil Using Portable Hand-Held Instruments*, Oak Ridge National Laboratory.

9. Sztajnkrycer, M. D. *Chemical and Radiological Toxicity of Depleted Uranium*, Military Medicine 169, 3:212, 2004.

10. Ziock, K. P.; Craig, W. W.; Fabris, L.; Lanza, R. C.; Gallagher, S.; Berthhold, K.P.H.; Madden, N. W. Large Area Imaging Detector for Long-Range Passive Detection of Fissile Material. *IEEE Transactions of Nuclear Science* **October 2004**, *51* (5).

11. Bikit, I.; Slivka, J.; Mrdja, D.; Zikic-Todorovic, N.; Curcic, S.; Varga, E.; Veskovic, M.; Conkic, L. Simple Method for Depleted Uranium Determination. *The Japan Society of Applied Physics* **2003**.

12. *American National Standard: Calibration and Usage of Sodium Iodide Detector Systems*, American national Institute of Standard Inc., Nov. 1980.

INTENTIONALLY LEFT BLANK.

Appendix A. High Purity Germanium (HPGe) Detector Calibration

This appendix describes a calibration process relevant to both NaI and HPGe detectors. The calibration includes processes for both energy calibration and efficiency calibration. The energy calibration matches the 16,000 channels inherent in the hardware to energy bins with a calibrated energy width depending on the amplification setting. The efficiency calibration matches counts identified by the germanium counter with actual number of photons of a particular energy, to the number that entered the region of the counter. For example, the range of a 2 MeV photon in Germanium is ~9.2 cm. The 7.5 cm long x 7.5 cm diameter Germanium detector does not stop all the photons in the detector. For instance, if the photon comes in at a grazing angle it will enter, created knock-on electrons, and exit before dumping all its energy. The result is a count that registers in a lower energy channel.

Table A-1 contains data from a series of check sources. In line 1 are the isotopes used in the process. The activity for each radioactive source is shown on line 2 in terms of micro-Curies(uCi), and in line 3 the number of decay events per second which is uCi times 3.7×10^{-4} decaying events per second. The distance between the source and the detector is 2.25" (shown in line 4). The intensity of the individual gamma lines per 100 decays (as documented in reference 3, is shown in line 6. From the source activity and and the referenced line intensity can be calculated, and shown in line 7. The measured counts from the detector are documented in line 9, with the resulting efficiency in line 10.

Table A-1. Table of radioactive sources that identifies gamma line energy, measured counts and expected counts.

Co57	Cs137	Cs137	Ba133	Cd109	Co57	Co57	Ba133	Ba133	Ba133	Na22	Cs137	Mn54	Co60	Na22	Co60				
0.1	0.945	0.945	0.85	0.261	0.1	0.1	0.85	0.85	0.85	0.261	0.945	0.136	0.723	0.261	0.723	uCi (see Moyer)			
14.4136	31.8	37.3	80.998	88.036	122.06	136.47	276.4	302.85	356	511	661	834.83	1173.2	1274.5	1332.5	keV			
2.25	2.25	2.25	2.25	2.25	2.25	2.25	2.25	2.25	2.25	2.25	2.25	2.25	2.25	2.25	2.25	in from src		63.59	sfc area
																		7.065	HPGe area
6.18	5.4	1.3	34	3.6	85.6	10.88	7.16	18.3	62	170	85.1	100	99.97	99.94	99.98	line intensity(see Heath)			
25.40667	209.79	50.505	1188.1	38.628	351.91	44.729	250.2	639.48	2167	1824	3306.1	559.11	2971.4	1072.4	2971.7	expected events/s			
7.7	61	16	327	10.3	100	12.5	31.3	75.5	231	242.5	190.8	33.6	91.6	59	82	measured events/s			
0.30307	0.290767	0.3168	0.2752	0.2666	0.2842	0.2795	0.1251	0.1181	0.107	0.08	0.0577	0.0601	0.0308	0.055	0.0276	efficiency			

The data from the table is shown in figure A-1, and fit to a third order polynomial. The data on the graph, reduced from the table is efficiency of the detector as determined by the number of counts under the line, not the peak of the centroid.

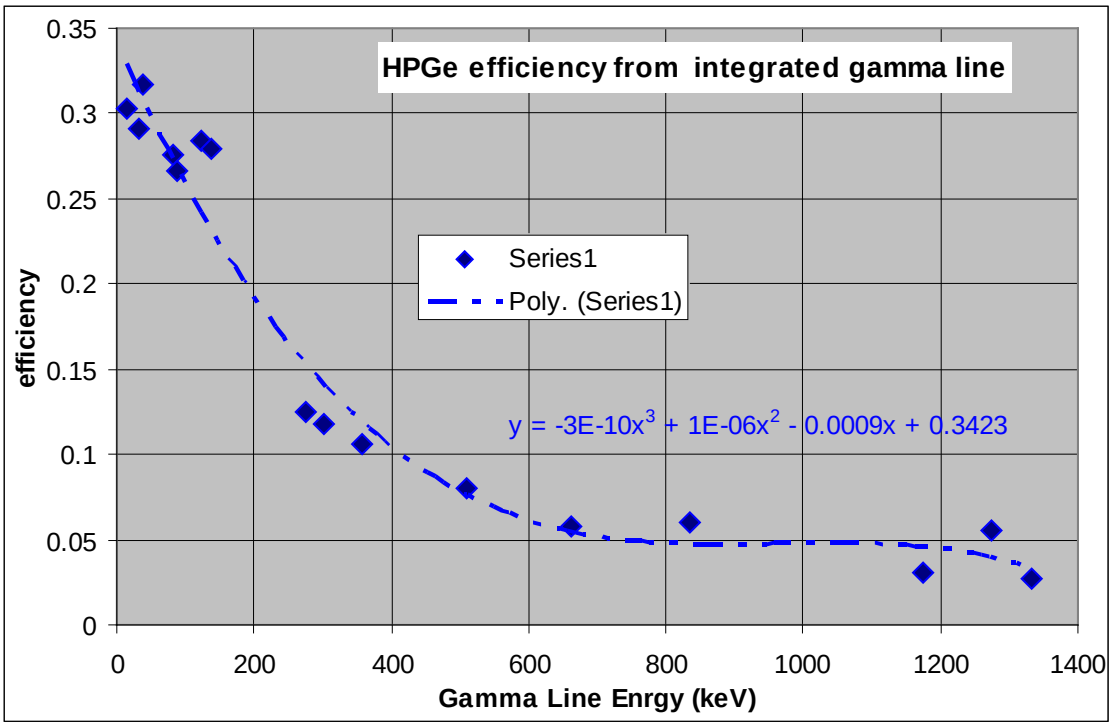

Figure A-1. Resulting efficiency calculated from the ratio of measured to expected accounts.

Appendix B. MATLAB Codes

This appendix contains the MATLAB codes used in the analysis of the raw experimental data as well as the integration of the NaI detector efficiency equation.

```
%% This program was made to read in and display various aspects of the
%% Depleted uranium data taken on May 15th, 17th and 21st.
%% Specifically the distance experiments

function DU_reader
suffix='.Spe';
b = 0 ; m=  1.42;
imax = 12;
DU1 = 1; DU2 = 400;

%file paths
%path{1} = '\\Datap\F\05_07\DU_May21\'; mult_offset=1;
path{2} = 'C:\Documents and Settings\All Users\Desktop\05_07\DU_May15\'; mult_offset=1;
path{1} = '\\Datap\F\05_07\DU_May15_and_17\'; mult_offset=1;

% interval for peak search
DU1 = 10; DU2 = 30;

%NaI
file{1} = 'DU_bkgnd.spe';
file{2} = 'DU_0cm.spe';
file{3} = 'DU_10cm.spe';
file{4} = 'DU_20cm.spe';
file{5} = 'DU_50cm.spe';
file{6} = 'DU_90cm.spe';
file{7} = 'DU_200cm.spe';
file{8} = 'DU_500cm.spe';
file{9} = 'DU_1000cm.spe';
%HPGe
file{10} = 'DU_bkgnd.spe';
file{11} = 'DU_0cm.spe';
file{12} = 'DU_10cm.spe';
file{13} = 'DU_20cm.spe';
file{14} = 'DU_50cm.spe';
file{15} = 'DU_86cm.spe';

%% This loops over the files from the NaI detector
%% stats looks for and calculates the peak, a smoothing function was
%% created but was commented out as it was deemed un-necessary

k=1;
for j = 2:9
[ENaI,c,nc,lt,rt,dE,E0,ch]=ASC_ortec_sdata2([path{k},file{j}]);
counts(:,j)=c;
cpsNaI(:,j)=c/lt;
totalCounts(j)=nc;
live(j)=lt;  dt(j) = (rt-lt)/rt;
%[c]=smooth2(c,3);
%figure{90 + j},
[pk,fw,ris,Emag,xpk] = stats(ch,c,DU1,DU2);
```

```
fw
xpk2 = xpk(1);
xvalpk(j)=xpk2;
cpk(j) = pk(1);
ch1 = ch;
ChanPk(j)=xpk(1);
fwval(j)=abs(fw);
realCounts(j) = sum(counts(abs(ChanPk(j)-fwval(j)/2-mod(ChanPk(j)-fwval(j)/2,1)):abs(ChanPk(j)+fwval(j)/2-
mod(ChanPk(j)+fwval(j)/2,1)),j));
end;

% changes NaI channel numbers to energies based on NaI calibration
Erange = dE*ch1 + E0;

% changes channel number found with highest numberof counts into energy
%based on NaI calibration
Epk = xvalpk*dE + E0;


%% This loops over the files from the HPGe detector
%% stats looks for and calculates the peak, a smoothing function was
%% created but was commented out as it was deemed un-necessary
k = 2;
for j = 10:15
[ENaI,c,nc,lt,rt,dE,E0,ch]=ASC_ortec_sdata2([path{k},file{j}]);
counts2(:,j-9)=c;
cpsNaI2(:,j-9)=c/lt;
totalCounts(j)=nc;
live(j)=lt;  dt(j) = (rt-lt)/rt;
%[c]=smooth2(c,3);
%figure{90 + j},
[pk,fw,ris,Emag,xpk] = stats(ch,c,DU1,DU2);
xpk2 = xpk(1);
xvalpk2(j-9)=xpk2;
cpk(j) = pk(1);
xpk = 0;
ch2 = ch;
end;

% changes HPGe channel numbers to energies based on HPGe calibration
Erange2 = dE*ch2 + E0;
Epk2 = xvalpk2*dE + E0

%used to plot data againest (x components)
A1 = 1:imax;
A2 = [0,10,20,50,100,200,500,1000];
A3 = [0,10,20,50,86];

% these are left here in case numbers are needed instead of just plots

%looking for standard deviation for each file
stdev = sqrt(counts);
stdev2 = sqrt(counts2);
realCounts

%%%%%%%%%%%%%%%%%%%%%% PLOTS

%%% highest peak of counts found for NaI
figure(1)
plot(A2,Epk(2:9),'r+')
 title(['NaI DU Data (Peak if highest counts)' ]);
xlabel('Distance'); ylabel('Peak of total Counts');
```

```
%xlim([-5,100])
grid on;

%%% highest peak of counts found for HPGe
figure(2)
plot(A3,Epk2(2:6),'r+')
 title(['HPGe DU Data (Peak of highest counts)' ]);
xlabel('Distance'); ylabel('Energy Peak of highest Counts');
grid on;

%%% dead time for NaI
figure(3)
plot(A2,dt(2:9),'r+')
 title(['NaI DU Data (Dead Time/Distance)' ]);
xlabel('Distance'); ylabel('Dead Time');
grid on;

%%% dead time for HPGe
figure(4)
plot(A3,dt(11:15),'r+')
title(['HPGe DU Data (Dead Time/Distance)' ]);
xlabel('Distance'); ylabel('Dead Time');
grid on;


%%% total Counts for NaI
figure(5)
semilogy(A2,totalCounts(2:9),'r+')
title(['NaI DU Data (Total Counts/Distance)' ]);
xlabel('Distance'); ylabel('Total Counts');
grid on;


%%% total Counts for HPGe
figure(6)
semilogy(A3,totalCounts(11:15),'r+')
title(['HPGe DU Data (Total Counts/Distance)' ]);
xlabel('Distance'); ylabel('Total Counts');
grid on;


%%% total spectrum NaI
figure(7)
semilogy(Erange,counts)
title(['NaI DU Data (Energy Spectrum)' ]);
xlabel('Energy'); ylabel('Counts');
legend([file]);
grid on;


%%% total spectrum HPGe
figure(8)
semilogy(Erange2,counts2)
title(['HPGe DU Data (Energy Spectrum)' ]);
xlabel('Energy'); ylabel('Counts');
legend([file]);
%xlim([1600,2000]); % <-- Adding this statement and modifying the plotting statement
                    % allows you to parse out the HPGe plot to better identify
                    % specific energies
grid on;
```

```
%%% counts in peak NaI
figure(9)
semilogy(A2,cpk(2:9),'r+')
title(['NaI DU Data (Highest Energy Peak Counts)' ]);
xlabel('Distance'); ylabel('Counts of highest Peak');
grid on;


%%% counts in peak HPGe
figure(10)
semilogy(A3,cpk(11:15),'r+')
title(['HPGe DU Data (Highest Energy Peak Counts)' ]);
xlabel('Distance'); ylabel('Counts of highest Peak');
grid on;
dt
xvalpk

%%%NaI vs. HPGe
figure(11)
hold on;
semilogy(Erange2,counts2(:,3))
plot(Erange,counts(:,3))
title(['NaI  and HPGe 10cm DU Data (Energy Spectrum)' ]);
xlabel('Energy'); ylabel('Counts');
hold off
grid on;


%% This function analyzes the Time experiment data for location of DU
function DU_reader_time
suffix='.Spe';
b = 0 ; m=  1.42;
imax = 12;
DU1 = 1; DU2 = 400;

%% file path
path{1} = 'L:\AltEn Team\Photon Counting\DU examination\DU Data\DU_May15_and_17\may 18\'; mult_offset=1;



% files
DU1 = 1; DU2 = 2000;
%NaI
file{1} = 'DU_15s_1000cm.spe';
file{2} = 'DU_30s_1000cm.spe';
file{3} = 'DU_60s_1000cm.spe';
file{4} = 'DU_120s_1000cm.spe';
file{5} = 'DU_1000cm.spe';
file{6} = 'DU_30min_1000cm2.spe';
file{7} = 'DU_15s_reversed.spe';
file{8} = 'DU_30s_reversed.spe';
file{9} = 'DU_60s_reversed.spe';
file{10} = 'DU_120s_reversed.spe';
file{11} = 'DU_reversed.spe';
file{12} = 'DU_30min_1000cm_reversed2.spe';
file{13} = 'DU_LeadCase_15s.spe';
file{14} = 'DU_LeadCase_30s.spe';
file{15} = 'DU_LeadCase_1min.spe';
file{16} = 'DU_LeadCase_2min.spe';
file{17} = 'DU_LeadCase_3min.spe';
%file{17} = 'DU_LeadCase_5min.spe';
file{18} = 'DU_LeadCase_30min.spe';
```

```
%% places information from the Scintivision output files into arrays which
%% can be manipulated in this loop and outside it as well
for j = 1:18
[ENaI,c,nc,lt,rt,dE,E0,ch]=ASC_ortec_sdata2([path{1},file{j}]);
counts(:,j)=c;
cpsNaI(:,j)=c/lt;
totalCounts(j)=nc;
live(j)=lt;  dt(j) = (rt-lt)/rt;
[pk,fw,ris,Emag,xpk] = stats(ch,c,DU1,DU2);
xpk2 = xpk(1);
xvalpk(j)=xpk2;
cpk(j) = pk(1);
ChanPk(j)=xpk(1);
fwval(j)=abs(fw);
realCounts(j) = sum(counts(abs(ChanPk(j)-fwval(j)/2-mod(ChanPk(j)-fwval(j)/2,1)):abs(ChanPk(j)+fwval(j)/2-
mod(ChanPk(j)+fwval(j)/2,1)),j));
xpk = 0;
ch1 = ch;
end;

%% these use the energy calibration of the detector for plotting the data
Erange = dE*ch1 + E0;
Epk = xvalpk*dE + E0

%% these arrays are used for plotting purposes
A2 = [15,30,60,120,180,1800];
A3 = [15,30,60,120,180,1800,15,30,60,120,180,1800,15,30,60,120,180,1800];

%looking for standard deviation for each file
stdev = sqrt(counts);









%%%%%%%%%%%%%%%%%%%%%%%% PLOTS %%%%%%%%%%%%%%%%%%%%%%%%%%%%%%%%%%%%%%%%

%%% highest peak of counts found for NaI
figure(1)
plot(A2,Epk(1:6),'r+')
 title(['NaI DU Data (Peak if highest counts)' ]);
xlabel('Distance'); ylabel('Peak of total Counts');
%xlim([-5,100])
grid on;


%%% dead time for NaI
figure(3)
plot(A2,dt(1:6),'r+')
 title(['NaI DU Data (Dead Time/Distance)' ]);
xlabel('Distance'); ylabel('Dead Time');
grid on;


%%% total Counts for NaI
figure(5)
hold on
```

```
semilogy(A2(1:5),totalCounts(1:5),'r+')
semilogy(A2(1:5),totalCounts(7:11),'r+')
semilogy(A2(1:5),totalCounts(13:17),'r+')
hold off
title(['NaI DU Data (Total Counts vs. Run Time)' ]);
xlabel('Time(sec)'); ylabel('Total Counts');
legend('Facing DU', 'Away from DU', 'Lead Encased')
grid on;



%%% total spectrum NaI
figure(7)
semilogy(Erange,counts)
title(['NaI DU Data (Energy Spectrum)' ]);
xlabel('Energy'); ylabel('Counts');
legend([file]);
grid on;

%%% total spectrum NaI
figure(10)
semilogy(Erange,counts(:,6:6:18))
title(['NaI DU Data 30 min(Energy Spectrum)' ]);
xlabel('Energy'); ylabel('Counts');
grid on;


%%% counts in peak NaI
figure(9)
semilogy(A2(1:6),cpk(1:6))
semilogy(A2(1:6),cpk(7:12))

title(['NaI DU Data (Highest Energy Peak Counts/Run Time)' ]);
xlabel('Distance'); ylabel('Counts of highest Peak');
grid on;


 %% This program reads in and analyzes either the unshielded DU directional
%% data or the shielded depending on the users preference

function DU_reader_direction
suffix='.Spe';
b = 0 ; m=  1.42;
imax = 12;
DU1 = 1; DU2 = 400;

%% file path
path{1} = '\\Datap\F\06_07\DU Directionality\DU_Direct_June27\'; mult_offset=1;
%path{1} = '\\Datap\F\06_07\DU Directionality\DU_Direct_Unshielded_June28\'; mult_offset=1;



% files
DU1 = 1; DU2 = 2000;
%NaI
file{1} = '0deg_shielded.spe';
file{2} = '45deg_shielded.spe';
file{3} = '90deg_shielded.spe';
file{4} = '135deg_shielded.spe';
file{5} = '180deg_shielded.spe';
file{6} = '225deg_shielded.spe';
file{7} = '270deg_shielded.spe';
```

```
file{8} = '315deg_shielded.spe';


% file{1} = '0deg_unshielded.spe';
% file{2} = '45deg_unshielded.spe';
% file{3} = '90deg_unshielded.spe';
% file{4} = '135deg_unshielded.spe';
% file{5} = '180deg_unshielded.spe';
% file{6} = '225deg_unshielded.spe';
% file{7} = '270deg_unshielded.spe';
% file{8} = '315deg_unshielded.spe';


%% places information from the Scintivision output files into arrays which
%% can be manipulated in this loop and outside it as well
for j = 1:8
[ENaI,c,nc,lt,rt,dE,E0,ch]=ASC_ortec_sdata2([path{1},file{j}]);
counts(:,j)=c;
cpsNaI(:,j)=c/lt;
totalCounts(j)=nc;
live(j)=lt;  dt(j) = (rt-lt)/rt;

[pk,fw,ris,Emag,xpk] = stats(ch,c,DU1,DU2);
xpk2 = xpk(1);
xvalpk(j)=xpk2;
cpk(j) = pk(1);
ChanPk(j)=xpk(1);
fwval(j)=abs(fw);
realCounts(j) = sum(counts(abs(ChanPk(j)-fwval(j)/2-mod(ChanPk(j)-fwval(j)/2,1)):abs(ChanPk(j)+fwval(j)/2-
mod(ChanPk(j)+fwval(j)/2,1)),j));
xpk = 0;
ch1 = ch;
end;

%% these use the energy calibration of the detector for plotting the data
Erange = dE*ch1 + E0;
Epk = xvalpk*dE + E0

%% these arrays are used for plotting purposes
A2 = [0,45,90,135,180,225,270,315];
A3 = [0,pi/4,pi/2,3*pi/4,pi,5*pi/4,3*pi/2,7*pi/4,0];

%looking for standard deviation for each file
stdev = sqrt(counts);




%%%%%%%%%%%%%%%%%%%%%%%% PLOTS %%%%%%%%%%%%%%%%%%%%%%%%%%%%%%%%%%%%%%%

%%% highest peak of counts found for NaI
figure(1)
plot(A2,Epk(1:8),'r+')
 title(['NaI DU Data (Highest Peak of counts)' ]);
xlabel('Degree off DU target'); ylabel('Highest Peak of  Counts (keV)');
grid on;

figure(12)
polar(A3,[cpk,cpk(1)])
 title(['NaI DU Data (Counts in Highest Peak)' ]);
xlabel('Degree off DU Target'); ylabel('Counts');
```

```
grid on;

figure(9)
polar(A3,[totalCounts,totalCounts(1)])
 title(['NaI DU Data (Total Counts)' ]);
xlabel('Degree off DU Target'); ylabel('Total Counts');
grid on;

figure(10)
polar(A3,[realCounts,realCounts(1)])
 title(['NaI DU Data (FWHM Counts in Highest Peak)' ]);
xlabel('Degree off DU Target'); ylabel('FWHM Counts');
grid on;

% plot of counts vs. channel
figure(5)
semilogy(ch,counts)
   grid on;
   title(['NaI DU Data (Channel)' ]);
   xlabel('Channel'); ylabel('Counts');
   legend([file])

% plot of energy vs. counts/sec
figure(6)
plot(Erange,counts)
   grid on;
   title(['NaI DU Data [Energy]' ]);
   xlabel('Energy (keV)'); ylabel('Counts');
   legend([file])


function pointsource_efficiency
%% Computes NaI detector efficiency at absorbing gamma radiations
%% Based on an equation found in Scintillation Spectrometry: Gamma-Ray
%% Spectrum Catalogue, by R.L. Heath
%% Tau values are based on fits to an absorption coeeficient graph found in
%% The Atomic Nucleus, by R. D. Evans

%%These values are the dimensions of the detector and the distance from
%%detector to source
h0 = 1;
t0 = 5.08;
r0 = 2.54;

kmax = 500;
c1 = atan(r0/(h0+t0));
c2 = atan(r0/h0);
T0=0;

dth1 = (c1-0)/(kmax-1);
dth2 = (c2-c1)/(kmax-1);

%%Loops over absorption coefficient based on energy and solves the integral
%%from Heath using a simple integration scheme
j=0;
for i = 1:7000
    j = j + 0.2;
    Ept(i) = j;
    if(j <35)
        tau(i) = 3.67*(171125*(j.^-3.0706));
    elseif(j>=35 && j<=200)
        tau(i) = 3.67*(472607*(j.^-2.7501));
```

```
    elseif(j>200 && j<=400)
        tau(i) = 3.67*(33657*(j.^-2.2415));
    elseif(j>400 && j<=1000)
        tau(i) = 3.67*(2.835*(j.^-0.6814));
    else
        tau(i) = 3.67*(0.1017*(j.^-0.1974));
    end;
    theta1 = 0;
    theta2 = c1;
    for k = 1:kmax
        %% the two halves of the Heath equation
        T1(k) = (1-exp(-tau(i)*t0/cos(theta1)))*sin(theta1)*dth1;
        T2(k) = (1-exp(-tau(i)*(r0/sin(theta2) - h0/cos(theta2))))*sin(theta2)*dth2;
        theta1 = theta1 + dth1;
        theta2 = theta2 + dth2;
    end;

    T(i) = 0.5*(sum(T1) + sum(T2));
end;
E = 0.2:0.2:1400;

%% plots efficency versus energy
figure(66)
plot(E,T)
grid on
    title(['Total Absolute Efficiency Approximation' ]);
    xlabel('Energy (keV)'); ylabel('Efficiency');


%%Displays detector dimensions integrated over
x = t0./2.54;
y = r0*2/2.54;
disp(['NaI Detector Dimensions : ' num2str(x) ' x ' num2str(y)])

%%Display specific energies
disp(['Isotope  :  En Peak  :  NaI Eff'])
    disp(['----------------------------------------'])
    disp(['DU  :  94   :  ' num2str(T(470))])
```

(NaI DU Measurements_Jerome_T_Mlack_Nov07_2.doc)

No. of Copies	Organization
1 ELECT	ADMNSTR DEFNS TECHL INFO CTR ATTN DTIC OCP 8725 JOHN J KINGMAN RD STE 0944 FT BELVOIR VA 22060-6218
1	DARPA ATTN IXO S WELBY 3701 N FAIRFAX DR ARLINGTON VA 22203-1714
1 CD	OFC OF THE SECY OF DEFNS ATTN ODDRE (R&AT) THE PENTAGON WASHINGTON DC 20301-3080
1	US ARMY RSRCH DEV AND ENGRG CMND ARMAMENT RSRCH DEV AND ENGRG CTR ARMAMENT ENGRG AND TECHNLGY CTR ATTN AMSRD AAR AEF T J MATTS BLDG 305 ABERDEEN PROVING GROUND MD 21005-5001
1	PM TIMS, PROFILER (MMS-P) AN/TMQ-52 ATTN B GRIFFIES BUILDING 563 FT MONMOUTH NJ 07703
1	US ARMY INFO SYS ENGRG CMND ATTN AMSEL IE TD A RIVERA FT HUACHUCA AZ 85613-5300

No. of Copies	Organization
1	COMMANDER US ARMY RDECOM ATTN AMSRD AMR W C MCCORKLE 5400 FOWLER RD REDSTONE ARSENAL AL 35898-5000
1	US GOVERNMENT PRINT OFF DEPOSITORY RECEIVING SECTION ATTN MAIL STOP IDAD J TATE 732 NORTH CAPITOL ST NW WASHINGTON DC 20402
1	US ARMY RSRCH LAB ATTN RDRL CIM G T LANDFRIED BLDG 4600 ABERDEEN PROVING GROUND MD 21005-5066
18	US ARMY RSRCH LAB ATTN IMNE ALC HRR MAIL & RECORDS MGMT ATTN RDRL CIM L TECHL LIB ATTN RDRL CIM P TECHL PUB ATTN RDRL SED E J BRENT ATTN RDRL SED E J RUSSO ATTN RDRL SED E M LITZ (10 COPIES) ATTN RDRL SED E M BERRY ATTN RDRL SED E B ATKINSON ATTN RDRL SER M E ADLER ADELPHI MD 20783-1197

TOTAL: 27 (25 HCS, 1 CD, 1 ELECT)